CHEMISTRY OF MATERIALS

pubs.acs.org/cm

Article

What Can We Learn about PEDOT:PSS Morphology from Molecular Dynamics Simulations of Ionic Diffusion?

Published as part of the Chemistry of Materials virtual special issue "In Honor of Prof. Elsa Reichmanis".

Tahereh Sedghamiz,[#] Aleksandar Y. Mehandzhiyski,[#] Mohsen Modarresi,[#] Mathieu Linares, and Igor Zozoulenko*

Cite This: *Chem. Mater.* 2023, 35, 5512–5523

Read Online

ACCESS | Metrics & More | Article Recommendations | Supporting Information

ABSTRACT: Poly(3,4-ethylenedioxythiophene) polystyrene sulfonate (PEDOT:PSS) is one of the most important mixed electron-ion conducting polymers, where the efficiency of the ion transport is crucial for many of its applications. Despite the impressive experimental progress in the determination of ionic mobilities in PEDOT:PSS, the fundamentals of ion transport in this material remain poorly understood, and the theoretical insight into the ion diffusion on the microscopical level is completely missing. In the present paper, a Martini 3 coarse-grained molecular dynamics (MD) model for PEDOT:PSS is developed and applied to calculate the ion diffusion coefficients and ion distribution in the film. We find that the ion diffusion coefficients for Na^+ ions are practically the same in the PEDOT-rich and PSS-rich regions and do not show sensitivity to the oxidation level. We compare the calculated diffusion coefficients with available experimental results. Based on this comparison and based on the MD morphology simulation of PEDOT:PSS revealing the formation of pores inside the film, we revise a commonly accepted granular morphological model of PEDOT:PSS. Namely, we argue that PEDOT:PSS films, in addition to PEDOT-rich and PSS-rich regions, must contain a network of pores where the ion diffusion takes place.

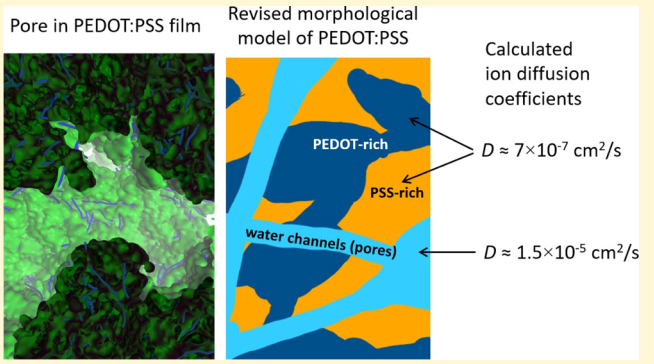

1. INTRODUCTION

Poly(3,4-ethylenedioxythiophene) polystyrene sulfonate (best known as PEDOT:PSS) is one of the most important and most studied conducting polymers. Its widespread use in organic and bioelectronics is because of the fact that it simultaneously possesses several important properties such as good environmental stability, well-developed synthesis routes, high electronic and ionic charge carrier mobilities, and tunable optical absorption (for reviews of various aspects of its material properties, see, e.g., refs 1−7). One of the essential features of PEDOT:PSS is that it is a mixed electron and ion conductor;[8−10] therefore, it can be used in a variety of applications requiring both electron and ion transport. These applications include supercapacitors and batteries,[11] electrochemical transistors[12,13] and biosensors,[14] neural probes and neuromorphic devices,[15] implantable drug delivery devices and ion pumps,[16] stretchable electronic devices,[17] and others.

In many of the abovementioned applications, the device's performance relies on the efficiency of the ion transport; therefore, during the past decade, the investigation of various aspects of ion transport in PEDOT:PSS has attracted great attention. In most of the reported studies, researchers mostly focused on the ionic conductivity σ (usually using impedance measurements),[18−22] whereas studies addressing the ion mobility μ (or the diffusion coefficient, $D = \mu k_B T/q$) are rather scarce.[23−25] (Note that determination of the mobility from the measured conductivity is typically not viable because the conductivity is the product of the ion charge, mobility, and concentration, $\sigma = q\mu n$, and the independent determination of the concentration of the ions contributing to the conductivity represents a significant challenge.) Direct measurement of the ion mobility in PEDOT:PSS was reported in the pioneering works of Malliaras and collaborators[23,24] who used the moving front experiments to monitor the electrochromic changes associated with the propagation of the dedoping front in the film. Recently, ion mobility measurements in PEDOT:PSS were performed using operando NMR spectroscopy.[25]

Despite of the impressive experimental progress in the determination of ionic mobilities in PEDOT:PSS, the

Received: April 13, 2023
Revised: June 1, 2023
Published: July 6, 2023

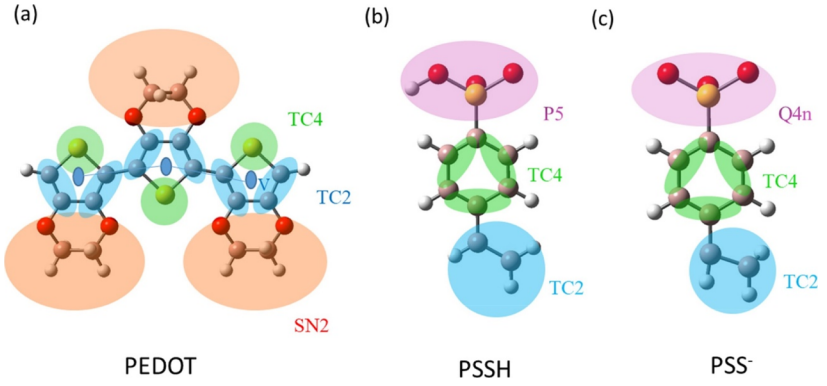

Figure 1. Martini 3 models of (a) PEDOT, (b) PSSH, and (c) PSS^- units.

fundamentals of ion transport in this material remain poorly understood, and the theoretical insight into the ion diffusion on the microscopical level is completely missing. There are several crucial questions awaiting their clarification, such as, "what is the theoretical value of the ion diffusion coefficient in PEDOT:PSS, and how this value is compared to the measured ones?" Another question is related to the microscopic picture of the ion diffusion and can be formulated as "where do ions move, in the PSS-rich or in PEDOT-rich regions, and what is the difference in the corresponding diffusion coefficients (if any)?" (Note that the presence of the PSS-rich and PEDOT-rich regions represents an essential morphological feature of PEDOT:PSS.) A further important question is "how does ion diffusion depend on the oxidation level?". Without understanding these questions, the comprehensive picture of the ion diffusion in PEDOT:PSS can hardly be properly built, and further improvement of materials and devices relying on mixed ionic and electronic transport in PEDOT:PSS can be difficult. Therefore, in the present paper, we aim to provide a comprehensive theoretical understanding of the ionic transport in PEDOT:PSS and to answer the above questions using molecular dynamics (MD) simulations.

During recent years, molecular modeling of conducting polymers, in particular, PEDOT, became a powerful tool not only complementing experimental studies but also providing essential theoretical insight and quantitative predictions of various aspects of the electronic, optical, transport, and morphological properties of the materials at hand. This includes simulation and modeling of optical properties,[26,27] morphology,[28−34] effects of solvents[35,36] and ionic liquids,[32,37] effect of substrate,[38] thermoelectric properties,[39−41] and electronic transport[33,42−44] (for a review, see ref 7). Calculations of ion diffusion were recently reported for PEDOT:tosylate[29] and mixed conducting polymers.[33] However, to the best of our knowledge, calculations of ion diffusion in PEDOT:PSS have never been attempted previously.

All-atom (AA) MD simulations represent a standard and well-developed technique to study the morphology and ion diffusion of many materials, including conducting polymers. However, because of computational limitations, AA MD simulations might not be suitable to describe realistically large systems, including PEDOT:PSS. Indeed, as mentioned above, PEDOT:PSS is characterized by a granular structure attributed to phase-separated PEDOT- and PSS-rich domains of the dimensions of 20−30 nm.[31] A computational box including domains of such sizes would be prohibitively large for the AA MD simulations. In order to circumvent such limitations, coarse-grained (CG) MD simulations are used, where several different atoms are combined in a single computational bead. One of the most popular CG MD models in the field of soft materials science and biomolecular systems is the Martini force field.[45,46] Recently, its refined version, Martini 3, was introduced, with an improved description of the interaction and introduced more versatile bead types.[47] In our previous studies, we reported the Martini 2 model for PEDOT:tosylate[29] and PEDOT:PSS.[31] In the present study, we develop and verify the Martini 3 model for PEDOT:PSS. Using the developed Martini 3 model and utilizing a granular model of PEDOT:PSS describing PEDOT- and PSS-rich regions developed in our previous study,[31] we calculate the diffusion coefficient in PEDOT:PSS at different oxidation levels and analyze spatial ion distribution using radial and spatial distribution functions (SDFs). We compare the calculated diffusion coefficients with available experimental results, and, based on this comparison, we revise a commonly accepted granular morphological model of PEDOT:PSS. Namely, we argue that PEDOT:PSS films, in addition to PEDOT-rich and PSS-rich regions, must contain a network of pores that forms during the drying process, where the ion diffusion takes place.

2. COMPUTATIONAL METHOD

2.1. Martini 3 Model for PEDOT:PSS. We investigate the morphology of PEDOT:PSS polymers and the dynamics of ions using the Martini 3 CG model.[47] In the previous Martini model (Martini 2), four atoms are mapped to a CG bead.[45] In Martini 3, new "small" and "tiny" beads are used for 2-to-1 and 3-to-1 mapping in addition to the standard 4-to-1 mapping of the Martini model. The interactions between CG beads are given by the 12-6 Lennard-Jones potentials, representing the nature of the underlying chemical groups. In the Martini model, there are four types of beads representing polar (P), intermediately polar (N), apolar (C), and charged (Q) potentials. Each of these types is divided into subtypes elucidating the hydrogen bonding capability of the particles: donor (d), acceptor (a), both donor and acceptor (da), and none (0), and degree of polarity with scales from 1 (low polarity) to 6 (high polarity). The selection of beads for a particular system is typically done by matching the free energy of transfer of the monomeric repeat unit, fitting the bond, and angle distribution of the corresponding atomistic system, and long-range structural properties such as the persistence length, radius of gyration, and end-to-end distance.

https://doi.org/10.1021/acs.chemmater.3c00873
Chem. Mater. 2023, 35, 5512−5523

The Martini 2 CG model for PEDOT:PSS was introduced in our previous study.[31] In the present study, we develop the PEDOT:PSS model based on the Martini 3 force field, as it provides improvements compared to the Martini 2 model. In the Martini 3 model, smaller bead sizes (tiny and small beads) are introduced to better represent groups such as ring-like fragments. This includes improvements in the description of $\pi-\pi$ stacking distance, as well as arrangements of the monomers within the chains as will be described below. To represent a PEDOT monomer, we use TC2, TC4, and SN2 beads as shown in Figure 1a. Following the Martini 2 model for PEDOT, a charged virtual site is introduced at the center of each thiophene ring with a charge of +0.33 e, which corresponds to a typical oxidation level of c_{ox} = 33%.[48] For the reduced PEDOT (c_{ox} = 0%), the charge on the virtual site is set to zero. The PEDOT chains are believed to be short, and the number of monomer units in a chain (the degree of polymerization, DP) is chosen to be 12.[49]

We modeled PSS and PSSH monomers with four Martini beads, including TC2, TC4, and Q4n/P5 as shown in Figure 1b,c. The Q4n bead is representative of a charged bead, and P5 is representative of an uncharged bead for the sulfonate group. The degree of polymerization of PSS is set to 50 monomers per chain. In the experimental material, the DP can exceed 1000. Modeling of such long chains is computationally expensive. Note that the chain length for DP = 50 greatly exceeds the persistence length of PSS, which justifies the utilization of the chosen chain length in the simulations. In particular, in our previous studies, we verified that the calculated morphologies for DP = 50 and DP = 2200 are the same for the case of a both single PEDOT:PSS particle and for the film.[31,50] The TQ5 CG bead type is used for modeling of Na^+ ions, and the W bead type is used for water molecules.[47] VMD is used for all molecular visualizations.[51]

In previous studies, single chain properties of polymers such as polystyrene, polyethylene, polyethylene oxide, and polypropylene were used for the parameterization of Martini CG models.[52−54] These properties included the persistence length l_p, the radius of gyration R_g, and the end-to-end distance d_{e-e}. To validate our model, we built the AA simulation model for the PSS and PEDOT molecules and compared the AA and CG results for l_p, R_g, and d_{e-e}, see Figure S1. The umbrella sampling method was used to validate the PEDOT beads. The details of the validation of PEDOT and PSS models are given in Section S1 in the Supporting Information. The list of all Lennard-Jones parameters used in the Martini 3 CG calculations is presented in Table S2. For the sake of reproducibility of our results, we provide a complete set of initial atomic positions, MD setup, and bonded and nonbonded interactions between beads in the Supporting Information (see Section S2).

It is noteworthy that the Martini 3 model provides an improved description of PEDOT:PSS films as compared to Martini 2. In particular, because of the utilization of "tiny" beads, the obtained $\pi-\pi$ stacking distance in PEDOT crystallites, $R_{\pi-\pi}$ = 0.36 nm (Figure S2), is consistent with the experiment and the AA calculations.[28] (Note that Martini 2 models overestimate the $\pi-\pi$ stacking distance in conducting polymers because the size of the beads used there is larger than $R_{\pi-\pi}$[55]). The Martini 3 model corrects another deficiency of Martini 2 concerning the arrangements of monomers in the PEDOT chain. Namely, another artifact of the Martini 2 model for PEDOT is that monomers belonging to neighboring chains in the crystallite face each other with the sulfur atoms pointing in the same direction. In the Martini 3 model, this deficiency is corrected, and the corresponding monomers point out in opposite directions, in accordance with the AA MD results,[28] see Figure S2b. Note that previously, this deficiency was corrected by the backmapping of the CG Martini morphology into the atomistic one.[56]

2.2. MD Simulations of the PEDOT:PSS Film. We use the model for the PEDOT:PSS thin film developed in our previous study,[31] and for the preparation of PEDOT:PSS thin film in water, we follow the main steps as described in this paper. These main steps consist of (a) preparation of the dried film; (b) immersing the dried film in water; and (c) deprotonation of PSSH, see Figure 2 for illustration. These steps are followed by (d) changing the oxidation level and (e) calculation of the diffusion coefficient. Step (f) describes a preparation of the dried film from two PEDOT:PSS particles to illustrate a pore formation. Based on the obtained morphology, the ion distribution in the film and ion diffusion are investigated. MD calculations in steps (a)-(e) are performed using the GROMACS package (version 5.0.4 2018a),[57] and step (f) is performed using the Gromacs 2022.2 version.[58]

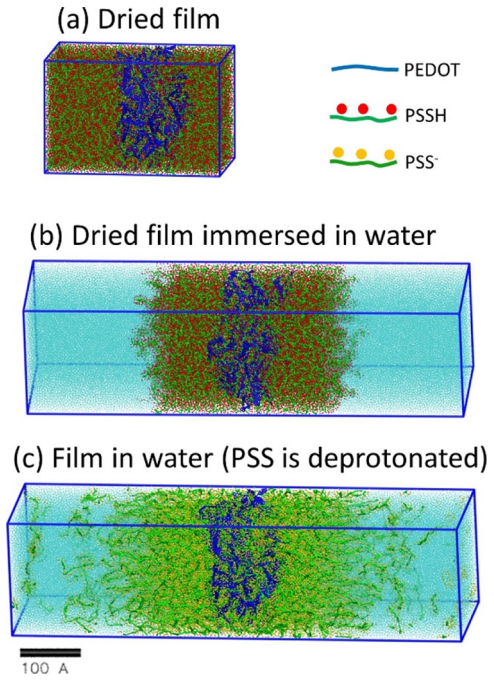

Figure 2. Preparation of PEDOT:PSS film immersed in water: (a) dried film; (b) immersing the dried film in water; (c) deprotonation of PSSH.

2.2.1. Preparation of the Dried Film. We use a model of PEDOT:PSS consisting of a core PEDOT-rich region surrounded by PSS-rich regions as shown in Figure S3. This can be considered as a "minimal model" of PEDOT:PSS because it captures the formation of PEDOT- and PSS-rich regions of realistic sizes (of the order of 15 nm in agreement with the experimental observations[1,2,5−7,24,31]).

More realistic models would include more PEDOT- and PSS-rich regions; however, such models are prohibitively computationally expensive even for CG MD approaches. The PEDOT-rich region consists of 1000 PEDOT and 200 PSS^-

https://doi.org/10.1021/acs.chemmater.3c00873
Chem. Mater. 2023, 35, 5512−5523

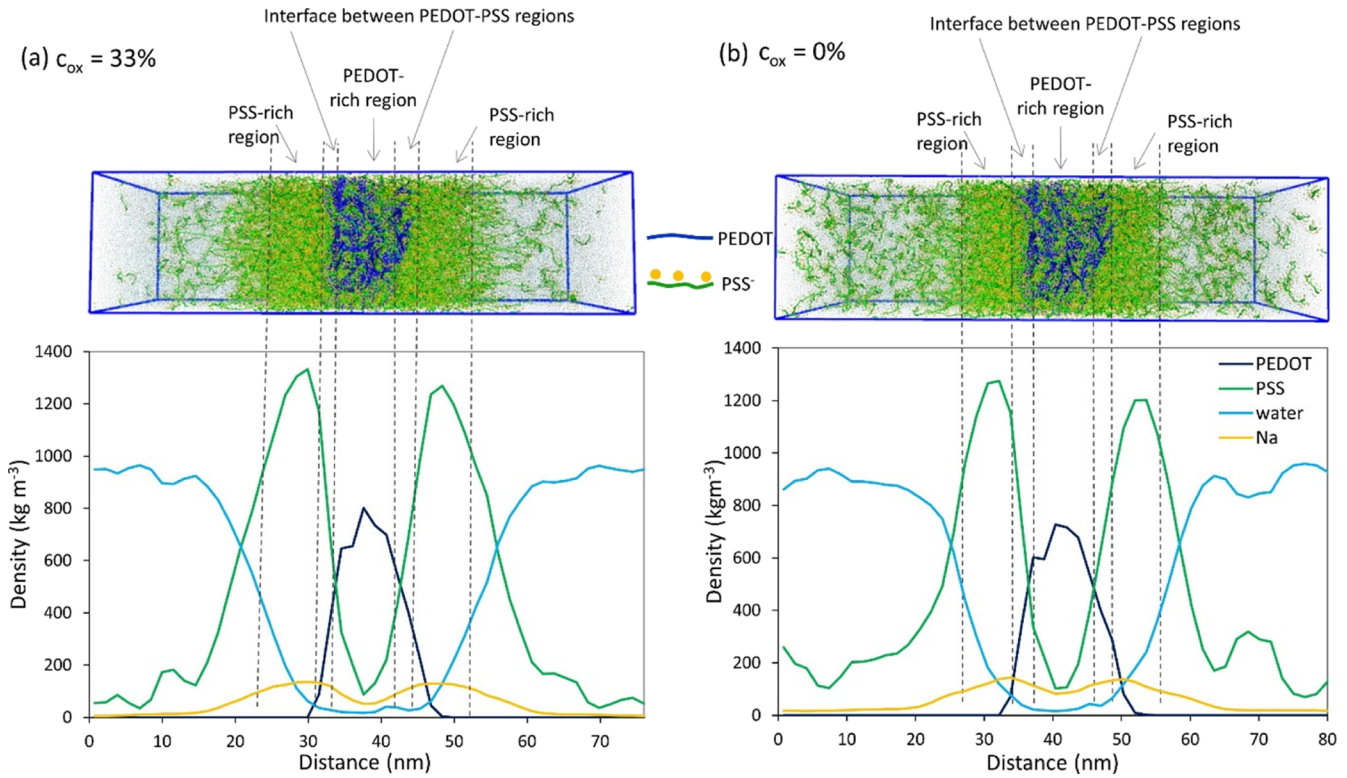

Figure 3. Density profiles of PEDOT, PSS, Na^+ ions, and water in PEDOT:PSS film for the oxidation level (a) c_{ox} = 33% and (b) c_{ox} = 0%. Dotted lines define PEDOT-rich, PSS-rich, and PEDOT−PSS interface regions. PEDOT- and PSS-rich regions are defined as those where the densities of PEDOT and PSS are approximately within 75% of their respective maximal values.

chains, where the ratio of protonated to deprotonated sulfonate groups on PSS is 1.65. There are 808 PSSH chains in the PSS-rich region. The initial simulation box dimension is 24 × 24 × 130 nm^3 and is filled with 587,000 Martini water molecules, corresponding to a 80% wt hydration level.

First, we make a solution of PEDOT:PSS with a 80% hydration level. Then the energy minimization is done by the steepest descent method and continued with an equilibration in the isothermal−isobaric ensemble (*NPT*) for 100 ns and the time step of 1 fs at 1 bar and 300 K using the velocity rescaling thermostat[59] and Berendsen barostat.[60] A restraint is applied to the polymer matrix during the equilibration process, and only water molecules freely move to uniformly fill the box space. In the production run (performed for 400 ns) the pressure is held constant at 1 bar by the Parrinello−Rahman barostat.[61] The choice of an *NPT* ensemble for the production run is to mimic the constant pressure and temperature in the laboratory condition. [Note that the same thermostats and barostats were used for equilibrations and production runs for steps (b−e) as well]. In all the MDs simulations, we use the smooth particle-mesh Ewald method to include the long-range electrostatic interaction.[62] The cutoff radius of electrostatic and vdW interactions is set to 1.2 nm.

Evaporation is done by randomly removing 10% of the remaining water at each step until reaching a dry film of 10% wt water (Figure S3). Note that because we remove 10% of the remaining water at each step, the absolute amount of removed water decreases with every step, and one requires 30 steps to dry a film from 80 to 10% wt hydration level. At each step, after removing 10% of water, the system is equilibrated for 8 ns, and a production run is performed for 10 ns in the *NPT* ensemble as specified above. The total MD simulation time during evaporation to reach the dried film is 18 ns × 30 steps = 540 ns. In the drying process, the pressure is applied semi-isotropically (isotropic in the x and y directions but variable in the z direction). We consider zero compressibility in the $x-y$ plane. As a result, the final dried film shrinks in the z direction, which mimics the thin film formation in the laboratory. The dimension of the final dried film is 20 × 20 × 40 nm^{-3}. Finally, we note that to save computational time, we used protonated PSS chains (i.e., PSSH). Strictly speaking, one should start with de-protonated chains and gradually protonate them during water evaporation. In previous simulations,[31] we observed that performing drying in both ways led to the same morphology. Therefore, to save computational time, we use the PSSH chain during the entire simulations.

2.2.2. Immersing the Dried Film in Water. Having prepared a dry film, we place it in water as illustrated in Figure 2b. The dimension of the computational box is 24 × 24 × 130 nm^{-3}. At the beginning of the simulation, the deprotonation level α, defining the relative ratio of the deprotonated sulfonate groups of PSS, is α = 0%, which means all the PSS molecules are protonated. (Note that, as discussed above, there are also some sulfonate groups in the PEDOT-rich region that are not completely protonated because they compensate for the positive charges of PEDOT, and they are not counted in the definition of α). The *NPT* equilibration is performed for 50 ns, where position restraints are applied on the polymer chains, followed by the *NPT* production run for 50 ns.

2.2.3. Deprotonation of PSSH. Placed in water, the film starts swelling as water molecules penetrate PSS-rich and PEDOT-rich regions and PSSH molecules become PSS^- step by step, as illustrated in Figure S4a. At each step, we deprotonated 20% of PSSH molecules by randomly replacing

https://doi.org/10.1021/acs.chemmater.3c00873
Chem. Mater. 2023, 35, 5512−5523

SO_3H units with SO_3^- and compensating for the negative charges by Na^+ ions. Na^+ ions are placed randomly in the computation box between water beads. We perform energy minimization and 30 ns *NPT* equilibration in the Berendsen barostat[60] to reach a proper starting point at each deprotonation step. [Note that the probability of deprotonation is higher for SO_3H units that are surrounded by a larger number of water molecules. For the sake of simplicity and computational efficiency, we do not account for this in our model because the re-arrangement of water molecules and protons (Na^+) due to fast diffusion takes place locally and is not expected to affect the long-range order].

Figure S5 shows the change in the number of Na^+ ions during deprotonation and the corresponding changes in the deprotonation and oxidation levels. At each step, the *NPT* equilibration is performed for 30 ns, where position restraints are applied to the polymer chains, followed by the *NPT* production run for 50 ns. (It is worth noting that an equilibration step is needed because Na^+ ions inserted between water beads experience a strong force from surrounding molecules, and we therefore need to reach a stable configuration before MD production run). Note that here, as in the previous study,[31] Na^+ ions play the role of H^+/H_3O^+ because a model for proton or hydronium in the Martini force field is not available yet. It is also noteworthy that in many experiments, Na^+ ions replace protons.[20] During the swelling process, the PEDOT-rich region width stays almost unchanged while the PSS-rich region expands from about 35−45 nm, see Figure S4b. Note that the swelling process and water intake in PEDOT:PSS are discussed in detail in our previous study.[31]

2.2.4. Changing the Oxidation Level. To prepare films with different oxidation levels, we start with a completely deprotonated system (α = 100%) and change the oxidation level of the PEDOT chains from c_{ox} = 33.3 to 0% in four steps: 33.3% → 25% → 16.8% → 8.3% → 0%. At each level, 1000 Na^+ ions were added to the water region of the system to compensate for the negative charges, see Figure S5. At each oxidation level, we performed a 30 ns *NPT* equilibration followed by 50 ns production run as described before.

2.2.5. Calculation of the Diffusion Coefficient. To calculate ion diffusion coefficients, 3000 Na^+ ions were randomly selected from each system. The ions situated closer than 0.43 nm to sulfonate-charged groups are considered as trapped, and they are not included in the calculations. The diffusion coefficient is calculated by the Einstein relation

$$D = \frac{\langle \Delta r^2(t) \rangle}{6t} \quad (1)$$

where $\Delta r^2(t)$ is the mean square displacement (MSD) of ions during the time interval t, and the averaging is performed over all selected ions. The diffusion coefficient is calculated in three regions in the simulation box (PEDOT-rich, PSS-rich, and PEDOT−PSS interface regions), which are defined based on the PEDOT and PSS density profiles, see Figure 3. The duration of the entire production run for the calculation of the MSDs is 10 ns. For each trajectory, we need to ensure that the ion stays in the chosen region. However, during the production run (10 ns), the ion can leave the region where it was initially situated. Therefore, we divide the entire trajectory into smaller intervals (2 ns), in which the ions typically stay in the same region (note that we check this during MSD calculations). Then, for each of these intervals, we calculate the MSD for every ion and use the obtained values to compute the diffusion coefficient according to eq 1.

It should be stressed that the diffusion coefficient given by eq 1 is properly defined only when the MSD depends linearly on time. To ensure that we are in the linear regime, we calculated the averaged MSDs for all ions, see Figure S6. Figure S6 also shows MSDs for different individual representative trajectories. While individual MSDs show deviations from the linear behavior, the average MSD exhibits almost perfect linear dependence. This clearly demonstrates the validity of eq 1 for our system. This also shows that our system is ergodic, that is an average over infinitely long time required in the definition of the diffusion coefficient eq 1 is equivalent to the averaging over many configurations (i.e., over many ion trajectories).

After this, the diffusion coefficients are calculated for another 1000 Na^+ ions, and the calculated results for all 4000 ions are compared to the results obtained in the previous step (for 3000 ions). This procedure (i.e., calculating the diffusion coefficient for 1000 more ions) continues until the calculated results (plotted as boxplots) do not change more than 3%.

2.2.6. Preparation of the Dried Film from Two PEDOT:PSS Particles to Illustrate Pore Formation. The same procedure as described in ref 31 was followed to obtain a dry film from PEDOT:PSS dispersion consisting of PEDOT:PSS particles. First, we prepare each PEDOT:PSS particle by randomly coiling a PSS chain (DP = 2200) around the PEDOT core, consisting of 100 oligomers with DP = 12. Then two such particles are placed in a periodic simulation box with dimensions 53 × 27 × 27 nm^3 and solvated with water molecules (N_{water} = 295,143). PEDOT:PSS is a highly stable water dispersion,[50] and therefore all sulfonated groups in our model are initially deprotonated. Second, the system is energy minimized with the conjugated gradient method and afterward equilibrated in the *NVT* (0.5 ns) and *NPT* (5 ns) ensembles at 300 K and 1 bar in the case of *NPT*. Finally, the water evaporation was done by removing approximately 1.2 wt % water beads (with respect to the weight of the entire simulation box, including PEDOT:PSS, water, and ions at the previous evaporation step) in 77 evaporation steps. The system was equilibrated between every two evaporation events for 0.5 ns in the *NVT* ensemble where the PEDOT:PSS particles were kept position restrained, which was then followed by another equilibration in the *NPT* ensemble for 5 ns utilizing the Berendsen barostat[60] with a coupling constant of 2 ps. The position restraints were applied only during the *NVT* runs to let water equilibrate better around the polymer chains and avoid sporadic movements of the chains due to the removed water molecules. The system was then simulated for an additional 10 ns under *NPT* conditions with the Parrinello−Rahman barostat at 1 bar with coupling constant of 4 ps. It should be noted that simulations with both isotropic and anisotropic pressure coupling were performed with compressibility of 0.0003 bar^{-1}. During water removal, PSS sulfonate groups were randomly protonated (under the condition that there was an Na^+ ion within 6 Å from them) to account for the decrease of the pH and the charge neutrality in the final dried film. This procedure was carried out until 10 wt % water was left in the box. The velocity rescaling thermostat[59] was used in all simulations with the coupling constant of 1 ps.

3. RESULTS AND DISCUSSION

We investigate the ion diffusion and ion distribution in the PEDOT:PSS thin film in water. We use the model for

https://doi.org/10.1021/acs.chemmater.3c00873
Chem. Mater. 2023, 35, 5512−5523

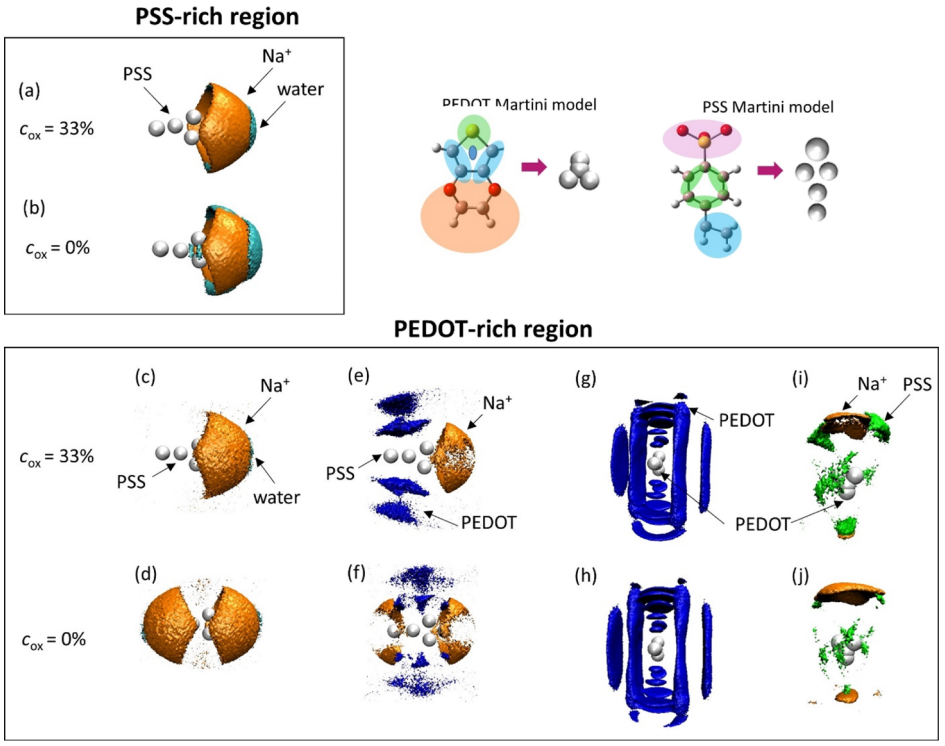

Figure 4. SDFs in (a,b) PSS-rich region, and (c−j) PEDOT-rich regions for oxidation levels c_{ox} = 33% and c_{ox} = 0%. SDFs are plotted for (a−d) PSS, Na^+, and water; (e,f) PSS, Na^+, and PEDOT; (g,h) PEDOT, Na^+, and PSS; (i,j) PEDOT−PEDOT. Insets in the upper right corner show visualization of PEDOT and PSS used in the SDFs.

PEDOT:PSS thin film developed in our previous study.[31] Within this model, PEDOT:PSS film immersed in water is a two-phase system consisting of PEDOT-rich and PSS-rich regions. The PEDOT-rich region consists of positively charged PEDOT chains compensated by negatively charged deprotonated PSS. The PEDOT-rich region consists of deprotonated PSS where protons or Na^+ ions compensate negatively charged sulfonate groups of PSS. Because of computational reasons, protons and Na^+ ions are treated on equal footing (they are described by the same Martini beads). To prepare the system, we follow a similar procedure as described in ref 31 and summarized in Figure 2. First, a dried PEDOT:PSS thin film is prepared (Figure 2a). Then the dried film is immersed in water (Figure 2b). In water, PSSH is de-protonated, and a final morphology is shown in Figure 2c. The details of the system preparation are described in the Computational Method section.

The densities of PEDOT, PSS, water, and ions in PEDOT- and PSS-rich regions are shown in Figure 3 for oxidized (c_{ox} = 33%) and fully reduced (c_{ox} = 0%) films. (PEDOT- and PSS-rich regions are defined as those where the density of PEDOT and PSS is approximately within 75% of their respective maximal value; the domain between these regions is defined as the interface region between the PEDOT- and PSS-rich regions). The density of Na^+ ions in the PSS-rich regions is larger than the PEDOT-rich region for both oxidized and reduced samples. This is because the density of PSS is larger in the PSS-rich regions. (Note that Na^+ ions compensate negatively charged sulfonate groups on PSS). By changing the oxidation level from 33 to 0%, Na^+ ions penetrate from the water region to the PEDOT-rich region to compensate for the negative charges of PEDOT chains. As a result, in a reduced PEDOT:PSS (c_{ox} = 0%), the number of ions in the PEDOT-rich regions increases by 60% as compared to the oxidized system (c_{ox} = 33%). During this process, the ions bring water with them which leads to the increase of the amount of water in the film.

To analyze the diffusion coefficients calculated in the present study, it is instrumental to understand the distribution of the ions in the system. In the present study, it is done with the help of the radial distribution functions (RDFs) and the SDFs, where the latter shows the probability of finding a particle at a certain position in space around a fixed reference system of other particles. Note that, in contrast to commonly used RDFs, SDFs are plotted in three dimensions and can involve more than two molecules. Figure 4 shows the SDFs for PEDOT, PSS, Na^+, and water in PEDOT-rich and PSS-rich regions at oxidation levels of c_{ox} = 33% and c_{ox} = 0%. The probability distributions are shown as isosurfaces (i.e., surfaces representing constant values of the probabilities). At each plot, isosurface values are chosen to be the same for each species so that we can compare densities of each species around a reference monomer. An alternative way to represent SDFs as contour maps is presented in Figure S7. The cut-off distance value of SDF plots is set to 10 Å for all plots (i.e., SDFs are plotted for species separated by up to 10 Å). All SDF plots are obtained by ViaMD software.[63,64]

Figure 4c,d shows the SDFs of PSS−Na^+−water for PSS- and PEDOT-rich regions for oxidized and reduced films (c_{ox} = 33% and c_{ox} = 0%, respectively), where PSS monomer is used as a reference unit, and Na^+ and water distributions are shown by orange and cyan isosurfaces, respectively. In all cases, the SDF exhibits a broad lobe wrapped around the charged bead of PSS, representing Na^+ ions attracted to negative sulfonate groups because of the Coulomb interaction. In addition, for the case of the PEDOT-rich region for the reduced PEDOT,

https://doi.org/10.1021/acs.chemmater.3c00873
Chem. Mater. 2023, 35, 5512−5523

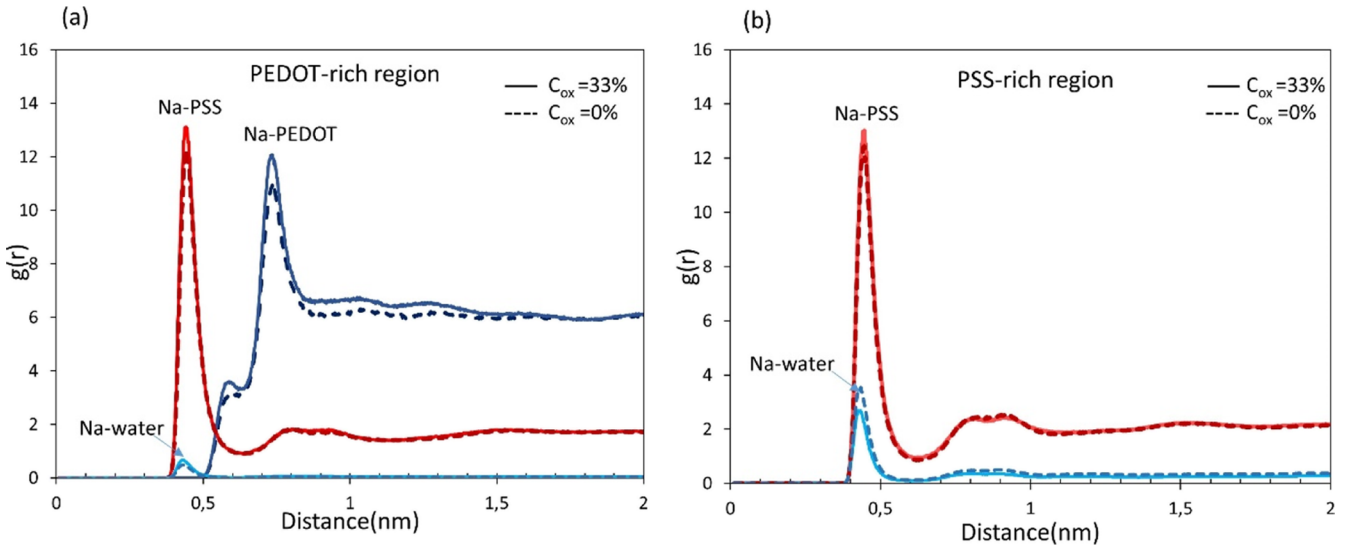

Figure 5. RDF $g(r)$ of Na^+ ions relative to PEDOT, PSS, and water molecules in the PEDOT-rich and PSS-rich regions for PEDOT oxidation levels equal to 33 and 0%. That is calculated based on the distance of Na^+ ions from the charged bead of PSS or the virtual bead of PEDOT.

the SDF distribution of Na^+ ions exhibits a second lobe (at the left part of the PSS unit in Figure 4d). This corresponds to Na^+ ions injected into the PEDOT-rich region during the reduction of PEDOT. Because all sulfonate groups are already compensated, the injected ions are distributed in the remaining available space around PSS. Figure 4a–d shows a spatial distribution of water, where the latter, as expected, is located close to Na^+ ions forming the hydration shells. In accordance with the density profiles presented in Figure 3, the amount of water is larger in the PSS-rich region, which is also reflected in the corresponding SDFs presented in Figure 4a–d. It is noteworthy that in both PEDOT- and PSS-rich regions, the amount of water surrounding PSS is larger for the reduced systems (c_{ox} = 0%) as compared to the oxidized one (c_{ox} = 33%), cf. Figure 4a,b. This is because during reduction, Na^+ ions injected into the film bring along water molecules in their hydration shells. Finally, Figure 4e,f provides the same information about the spatial distribution of Na^+ ions around PSS as Figure 4c,d, but in addition, they also show a spatial distribution of PEDOT, where the latter is primarily located around either side of PSS in its middle part. (Note that values of isosurfaces are different in Figure 4e,f and 4c,d). The SDFs for PSS–PSS are shown in Figure S8.

Let us now discuss the spatial distribution of PSS, PEDOT, and Na^+ around PEDOT. PEDOT–PEDOT spatial probability distribution exhibits vertical isosurfaces around a reference monomer in a PEDOT chain, see Figure 4g,h. This structure of isosurfaces apparently reflects a formation of $\pi-\pi$ stacking between PEDOT chains (note that the distance between the isosurfaces corresponds to the $\pi-\pi$ stacking distance $R_{\pi-\pi}$ = 0.36 nm obtained in the Martini model). The radial PEDOT–PEDOT distribution function, Figure S2c, shows four peaks at the multiples of the $\pi-\pi$ stacking distance $R_{\pi-\pi}$, which corresponds to five PEDOT chains in each crystallite in agreement with previous results.[31] The $\pi-\pi$ stacking distance $R_{\pi-\pi}$ between PEDOT chains does not show any differences by changing the oxidation level of PEDOT, cf. Figures 4g,h and S2c. The disk-like isosurfaces on top and bottom from the reference PEDOT monomer are the monomers belonging to the same chain. As the distance from the reference monomer increases, disks transform into the arks, which illustrates the bending (deviation from planarity) of PEDOT chains. (The bending of PEDOT chains in PEDOT:tosylate is discussed in ref 28). Because of the formation of $\pi-\pi$ stacked PEDOT crystallites, PSS is situated in the space surrounding these crystallites. This is manifested in SDFs of PEDOT–PSS, where PSS is situated close to the PEDOT backbone as well as on the top and bottom of the monomer (green clouds in the middle and the top and bottom of Figure 4i,j). Because of the electrostatic attraction, Na^+ surrounds the negatively charged sulfonate group of PSS.

Figure 5 shows the RDFs $g(r)$ for Na^+ ions with respect to PEDOT, PSS, and water at different oxidation levels (c_{ox} = 33% and c_{ox} = 0%) in PEDOT-rich and PSS-rich regions. The sharp and high peak in the RDF plot of Na^+–PSS at $r \approx 0.43$ nm (Figure 5a) is indicative of high correlation of ions with PSS as was seen in the SDFs in Figure 4a–d. The RDFs for Na^+–PEDOT show peaks at $r \approx 0.6$ and 0.7 nm. Their origin can be understood from the analysis of the corresponding SDFs: the first peak corresponds to Na^+ ions close to S in PEDOT monomers, whereas the second one corresponds to Na^+ ions on the opposite side of the monomers, see Figure 4i,j. The RDFs for Na^+–water show pronounced peaks at $r \approx 0.45$ nm, which reflects the formation of the hydration shells around ions.

Diffusion coefficients of Na^+ ions in three different regions of PEDOT:PSS film (PEDOT-rich, PSS-rich, and the interface) are shown in Figure 6 for oxidized and reduced films (c_{ox} = 33% and c_{ox} = 0%) in a form of boxplots. (The boxplots showing data through their quartiles are an efficient way for presenting the results when the data show a wide spreading. The MSDs are presented in Figure S6). The ion diffusion coefficients are practically the same in all three regions (with a median value $D \approx 7 \times 10^{-7}$ cm^2/s) and do not show sensitivity to the oxidation level. This result contrasts with the common belief that the ion diffusivity in the PSS-rich regions is larger than in the PEDOT-rich ones.[24] We relate the reason that the diffusion coefficient is rather similar in all three regions to the fact that the Na^+ distribution in the film is strongly correlated with PSS, which is hydrophilic and therefore represents a scaffold for the ionic motion. It is important to stress that PSS and water are present in both PSS- and PEDOT-rich regions,

https://doi.org/10.1021/acs.chemmater.3c00873
Chem. Mater. 2023, 35, 5512–5523

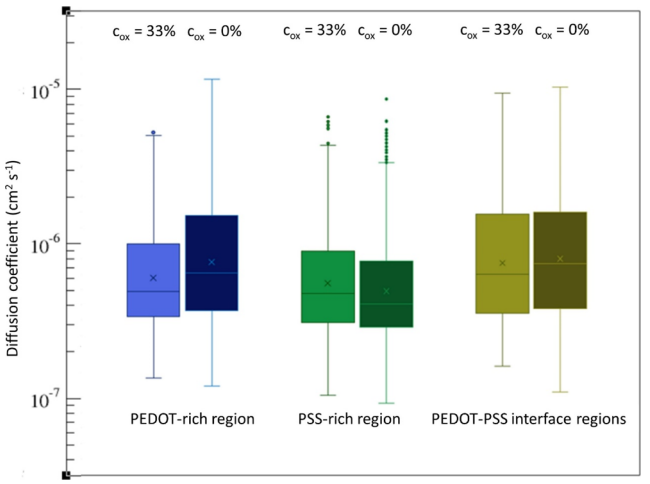

Figure 6. Boxplots of Na^+ ions diffusion coefficient in the PEDOT:PSS film in water for the oxidized and reduced films (c_{ox} = 33% and c_{ox} = 0%) for three different regions indicated in Figure 3 (PEDOT-rich, PSS-rich, and the interface). The boxplots present the data through their quartiles. In each boxplot, the average diffusion coefficient is indicated by "×" in the middle of the box; the horizontal line in each box indicates the median value. The vertical lines at the top and bottom of the boxes are the maximum and minimum values of each data set, respectively. Outliers (not included in the statistical analysis) are shown by dots.

and the Na^+−PSS distributions are practically the same in both regions (cf. Figure 5a,b; see also Figure 4a−d). Note, however, that ionic conductivity is expected to be significantly higher in the PSS-rich region because the ion concentration is much higher there (see Figure 3), and the conductivity is proportional to the product of the ion concentration and the diffusion coefficient.

There is a discussion in the literature on how the time scale of CG MD simulations and the corresponding calculated CG diffusion coefficient are related to the calculated AA MD diffusion coefficients and the experimental ones.[65] Our previous Martini 2 calculations for PEDOT:tosylate showed that CG diffusion coefficients matched rather closely the corresponding AA results. To establish this relation for the present system, we performed AA and Martini 3 simulations of Na^+ ion diffusion for a diluted PSS system, see Section S3 and Figure S9 for more details. We found that the corresponding diffusion coefficients are rather similar ($1.5 \pm 0.01 \times 10^{-5}$ and $1.7 \pm 0.01 \times 10^{-5}$ cm^2/s for Martini 3 and AA simulations, respectively). We also used CG Martini 3 to calculate the value of the Na^+ ion diffusion coefficient in pure water, which was $D = 1.22 \pm 0.03 \times 10^{-5}$ cm^2 s^{-1}. This value matches close to the experimentally measured value $D = 1.33 \pm 0.03 \times 10^{-5}$ cm^2 s^{-1}.[66] Based on this comparison, we conclude that calculated Martini 3 diffusion coefficients can be directly used for comparison to the experimental results.

Let us now compare our findings with available experimental results. The ionic mobilities in PEDOT:PSS were measured by Stavrinidou et al.[23,67] and Rivnay et al.[24] using moving front experiments. They found Na^+ mobilities to be $\mu = 0.93 \times 10^{-3}$ and $1.4–2.2 \times 10^{-3}$ cm^2/V s (corresponding to the diffusion coefficients $D = \mu k_B T/e = 2.8 \times 10^{-5}$ and $4.2–6.6 \times 10^{-5}$ cm^2/s, respectively, at T = 300 K). Lyu et al.[25] using nuclear magnetic resonance (NMR) measurement determined the diffusion coefficient for Na^+ ions in PEDOT:PSS $D = 1.13 \times 10^{-5}$ cm^2/s. The measured diffusion coefficients are close to the diffusion coefficient of Na^+ ions in pure water, $D = 1.33 \times 10^{-5}$ cm^2/s. (Surprisingly, the diffusion coefficients measured using the moving front experiments were even higher than those for pure water).

The calculated diffusion coefficients for Na^+ ions in PEDOT:PSS (with a median value $D \approx 7 \times 10^{-7}$ cm^2/s, see Figure 5) are significantly lower (by almost two orders of

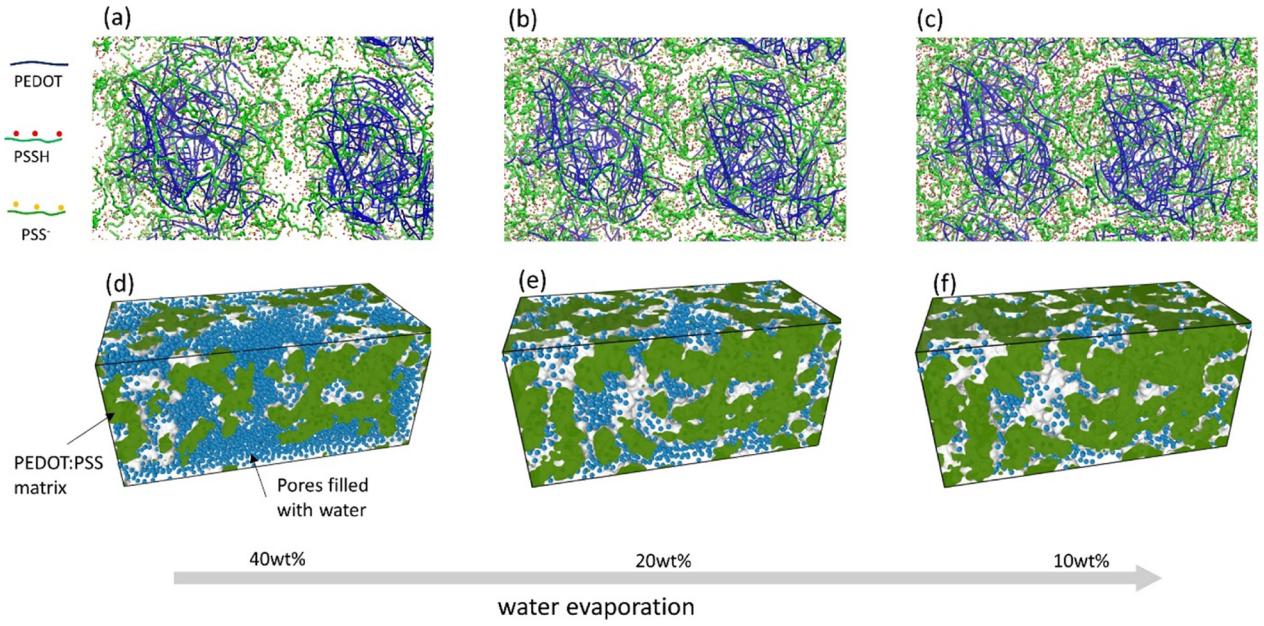

Figure 7. Simulation snapshots illustrating the formation of the PEDOT:PSS thin film from dispersion during drying for water content of (a) 40, (b) 20, and (c) 10 wt % under the condition of anisotropic pressure coupling. Snapshots (d−f) show the porous structure of the film (white regions) for different water content, where the water beads are shown as blue spheres. The green regions represent the PEDOT:PSS matrix defined as a surface with the density isovalue of 0.2.

https://doi.org/10.1021/acs.chemmater.3c00873
Chem. Mater. 2023, 35, 5512−5523

magnitude) than the abovementioned experimental values. At the same time, the calculated diffusion coefficients for Na^+ ions in diluted PSS and pure water match very well the experimental ones. This makes us to conclude that PEDOT:PSS films immersed in water must contain pores filled with water or water channels where ions move freely. Let us therefore discuss in more detail the formation of pores in PEDOT:PSS. (Note that pore formation in PEDOT:PSS was briefly mentioned in our previous study [see Figures S2 and S3 in ref 31], but its detailed investigation was left for future works).

As shown in our previous study,[31] PEDOT- and PSS-rich regions are formed during drying of the emulsion of PEDOT:PSS particles. Figure 7 illustrates the formation of PEDOT:PSS film starting with a system of two PEDOT:PSS particles. Each of the particles has a core−shell structure with a PEDOT-rich core (containing positively charged PEDOT and de-protonated PSS with negatively charged sulfonate groups compensating PEDOT charge) and a PSS-rich shell (composed primarily from de-protonated PSS chain and Na^+ or H^+ compensating the negative charge of sulfonate groups) (see for details ref 50). During drying, PSS protonates, and a thin film gradually forms, see Figure 7a−c, where the PEDOT-rich regions originate from the cores of the PEDOT:PSS particles, whereas PSS-rich regions originate from the shells. During the drying process and the thin film formation, voids (pores) appear in the film located in the space between the original dispersed particles, see Figure 7d−f. Note that we performed several independent simulations (varying also the evaporation rate, pressure coupling scheme or both simultaneously) of the film formation starting from PEDOT:PSS particles of similar sizes and shapes, and most of the simulations showed the presence of the pores inside the film, see Figure S10. Therefore, the calculated and measured ion diffusion coefficients in PEDOT:PSS combined with the MD simulations of PEDOT:PSS film formation strongly suggest the presence of pores (water channels) responsible for the fast ion-conductive pathways inside the film. We therefore propose a modified morphological model of PEDOT:PSS films where, in addition to PEDOT- and PSS-rich regions, the film contains a network of pores (water channels). When immersed in water, these pores are filled with water and support fast ion motion with the diffusion coefficient close to the one of pure water.

Note that in the present study, we focused on ion diffusion in thin films immersed in water. It is expected that in a dry film, the water is evaporated from pores and therefore the ionic diffusion would be greatly suppressed. Wieland et al.[20] studied the ionic conductivity of PEDOT:PSS films at different moisture levels. They showed that the ionic conductivity exponentially decreases by three orders of magnitude when the water content decreases from ≈80 to ≈10 wt %. In our previous studies of ion diffusion in the conducting polymer PEDOT:tosylate, we also found that the diffusion coefficients decreased exponentially by three orders of magnitude when the hydration level was varied from ≈80 to ≈10 wt %.[29] We attributed an exponential decrease of the diffusion coefficient in this system to the evolution of the water clusters that become fragmented into smaller and disconnected clusters and their sizes decrease exponentially as the water content decreases. We speculate that the behavior observed in PEDOT:PSS by Wieland et al.[20] can be caused by a similar reason when water is removed from pores and water clusters in the pores become disconnected that destroys percolative paths for ions. This, however, represents an interesting subject for further computational studies.

4. CONCLUSIONS

In the present paper, the Martini 3 CG model for PEDOT:PSS is developed and applied to calculate the ion diffusion coefficients. Ion distributions in various regions (PEDOT-rich and PSS-rich) and for various oxidation levels (fully oxidized and fully reduced) were analyzed using spatial and RDFs. We find that the ion diffusion coefficients for Na^+ ions are practically the same in the PEDOT-rich and PSS-rich regions (with a median value of $D \approx 7 \times 10^{-7}$ cm^2/s) and do not show sensitivity to the oxidation level. The calculated diffusion coefficients are significantly lower (by almost two orders of magnitude) than the experimentally measured ones. In their turn, the experimentally measured diffusion coefficients in PEDOT:PSS are close to those of pure water. Based on the calculated and measured ion diffusion coefficients in PEDOT:PSS and the simulation of PEDOT:PSS film revealing the formation of pores inside the film, we revise the morphological structure of PEDOT:PSS as follows. In contrast to practically all previous studies outlining the presence of PEDOT-rich and PSS-rich regions, we argue that PEDOT:PSS films, in addition, must contain a network of pores that forms during the drying process, see Figure 7d,e. When the film is immersed in water, the pores are filled in with water, which results in a fast and efficient ion transport with the diffusion coefficient close to that of pure water. We believe that our results demonstrate the power of the MD simulations for organic mixed electron-ion conductors, providing the essential insight into polymer morphology and ion diffusion that is difficult to obtain by other means.

■ ASSOCIATED CONTENT

Supporting Information

The Supporting Information is available free of charge at https://pubs.acs.org/doi/10.1021/acs.chemmater.3c00873.

Validation of Martini 3 PEDOT and PSS models; MD setups and parameters; AA and Martini diffusion calculations for the diluted PSS system; validation of PSS beads in Martini 3; Lennard-Jones parameters used in Martini 3 simulations; PMF from umbrella calculations; $\pi-\pi$ stacking of PEDOT chains; preparation of the dried film by water evaporation; PEDOT:PSS film in water for different deprotonation levels; change of the deprotonation and oxidation levels in the system due to addition of Na^+ ions; the SDFs represented as contour maps; the SDFs for PSS−PSS; calculated MDS; diluted PSS system for Martini 3 and all-atom MD calculations; and simulated morphology with isotropic pressure coupling and slower evaporation rate (PDF)

Files providing a complete set of initial atomic positions, MD setups, and bonded and nonbonded interactions between beads (ZIP)

■ AUTHOR INFORMATION

Corresponding Author

Igor Zozoulenko − *Laboratory of Organic Electronics (LOE), Department of Science and Technology (ITN), Linköping University, 60174 Norrköping, Sweden; Wallenberg Wood Science Center, Linköping University, 60174 Norrköping,*

https://doi.org/10.1021/acs.chemmater.3c00873
Chem. Mater. 2023, 35, 5512−5523

Sweden; orcid.org/0000-0002-6078-3006; Email: igor.zozoulenko@liu.se

Authors

Tahereh Sedghamiz − *Laboratory of Organic Electronics (LOE), Department of Science and Technology (ITN), Linköping University, 60174 Norrköping, Sweden*

Aleksandar Y. Mehandzhiyski − *Laboratory of Organic Electronics (LOE), Department of Science and Technology (ITN), Linköping University, 60174 Norrköping, Sweden;* orcid.org/0000-0001-5671-4545

Mohsen Modarresi − *Department of Physics, Faculty of Science, Ferdowsi University of Mashhad, 9177948974 Mashhad, Iran*

Mathieu Linares − *Group of Scientific Visualization, Department of Science and Technology (ITN), Linköping University, SE-60174 Norrköping, Sweden; Swedish e-Science Center (SeRC), Linköping University, SE-581 83 Linköping, Sweden;* orcid.org/0000-0002-9720-5429

Complete contact information is available at: https://pubs.acs.org/10.1021/acs.chemmater.3c00873

Author Contributions

#T.S., A.Y.M., and M.M. contributed equally.

Notes

The authors declare no competing financial interest.

■ ACKNOWLEDGMENTS

I.Z. acknowledges financial support from the Wallenberg Wood Science Center and the Knut and Alice Wallenberg Foundation (project "H_2O_2"). M.L. thanks the Swedish e-Science Research Centre (SeRC) for financial support. The computations were performed on resources provided by the National Academic Infrastructure for Supercomputing in Sweden (NAISS) at NSC, HPC2N, and PDC.

■ REFERENCES

(1) Elschner, A.; Kirchmeyer, S.; Lovenich, W.; Merker, U.; Reuter, K. *PEDOT: Principles and Applications of an Intrinsically Conductive Polymer*, 1st ed.; CRC Press, 2010; p 377

(2) Martin, D. C.; Wu, J.; Shaw, C. M.; King, Z.; Spanninga, S. A.; Richardson-Burns, S.; Hendricks, J.; Yang, J. The Morphology of Poly(3,4-Ethylenedioxythiophene). *Polym. Rev.* **2010**, *50*, 340−384.

(3) Shi, H.; Liu, C.; Jiang, Q.; Xu, J. Effective Approaches to Improve the Electrical Conductivity of PEDOT:PSS: A Review. *Adv. Electron. Mater.* **2015**, *1*, 1500017.

(4) Wen, Y.; Xu, J. Scientific Importance of Water-Processable PEDOT-PSS and Preparation, Challenge and New Application in Sensors of Its Film Electrode: A Review. *J. Polym. Sci., Part A: Polym. Chem.* **2017**, *55*, 1121−1150.

(5) Petsagkourakis, I.; Kim, N.; Tybrandt, K.; Zozoulenko, I.; Crispin, X. Poly(3,4-ethylenedioxythiophene): Chemical Synthesis, Transport Properties, and Thermoelectric Devices. *Adv. Electron. Mater.* **2019**, *5*, 1800918.

(6) Gueye, M. N.; Carella, A.; Faure-Vincent, J.; Demadrille, R.; Simonato, J.-P. Progress in Understanding Structure and Transport Properties of PEDOT-Based Materials: A Critical Review. *Prog. Mater. Sci.* **2020**, *108*, 100616.

(7) Zozoulenko, I.; Franco-Gonzalez, J. F.; Gueskine, V.; Mehandzhiyski, A.; Modarresi, M.; Rolland, N.; Tybrandt, K. Electronic, Optical, Morphological, Transport, and Electrochemical Properties of PEDOT: A Theoretical Perspective. *Macromolecules* **2021**, *54*, 5915−5934.

(8) Paulsen, B. D.; Tybrandt, K.; Stavrinidou, E.; Rivnay, J. Organic Mixed Ionic−Electronic Conductors. *Nat. Mater.* **2020**, *19*, 13−26.

(9) Berggren, M.; Crispin, X.; Fabiano, S.; Jonsson, M. P.; Simon, D. T.; Stavrinidou, E.; Tybrandt, K.; Zozoulenko, I. Ion Electron−Coupled Functionality in Materials and Devices Based on Conjugated Polymers. *Adv. Mater.* **2019**, *31*, 1805813.

(10) Keene, S. T.; Gueskine, V.; Berggren, M.; Malliaras, G. G.; Tybrandt, K.; Zozoulenko, I. Exploiting Mixed Conducting Polymers in Organic and Bioelectronic Devices. *Phys. Chem. Chem. Phys.* **2022**, *24*, 19144−19163.

(11) Sun, K.; Zhang, S.; Li, P.; Xia, Y.; Zhang, X.; Du, D.; Isikgor, F. H.; Ouyang, J. Review on Application of PEDOTs and PEDOT:PSS in Energy Conversion and Storage Devices. *J. Mater. Sci.: Mater. Electron.* **2015**, *26*, 4438−4462.

(12) Rivnay, J.; Inal, S.; Salleo, A.; Owens, R. M.; Berggren, M.; Malliaras, G. G. Organic Electrochemical Transistors. *Nat. Rev. Mater.* **2018**, *3*, 17086.

(13) Khau, B. V.; Scholz, A. D.; Reichmanis, E. Advances and Opportunities in Development of Deformable Organic Electrochemical Transistors. *J. Mater. Chem. C* **2020**, *8*, 15067−15078.

(14) Donahue, M. J.; Sanchez-Sanchez, A.; Inal, S.; Qu, J.; Owens, R. M.; Mecerreyes, D.; Malliaras, G. G.; Martin, D. C. Tailoring PEDOT Properties for Applications in Bioelectronics. *Mater. Sci. Eng., R* **2020**, *140*, 100546.

(15) Berggren, M.; Głowacki, E. D.; Simon, D. T.; Stavrinidou, E.; Tybrandt, K. In Vivo Organic Bioelectronics for Neuromodulation. *Chem. Rev.* **2022**, *122*, 4826−4846.

(16) Arbring Sjöström, T.; Berggren, M.; Gabrielsson, E. O.; Janson, P.; Poxson, D. J.; Seitanidou, M.; Simon, D. T. A Decade of Iontronic Delivery Devices. *Adv. Mater. Technol.* **2018**, *3*, 1700360.

(17) Zhang, G.; McBride, M.; Persson, N.; Lee, S.; Dunn, T. J.; Toney, M. F.; Yuan, Z.; Kwon, Y.-H.; Chu, P.-H.; Risteen, B.; Reichmanis, E. Versatile Interpenetrating Polymer Network Approach to Robust Stretchable Electronic Devices. *Chem. Mater.* **2017**, *29*, 7645−7652.

(18) Lefebvre, M.; Qi, Z.; Rana, D.; Pickup, P. G. Chemical Synthesis, Characterization, and Electrochemical Studies of Poly(3,4-Ethylenedioxythiophene)/Poly(Styrene-4-Sulfonate) Composites. *Chem. Mater.* **1999**, *11*, 262−268.

(19) Wang, H.; Ail, U.; Gabrielsson, R.; Berggren, M.; Crispin, X. Ionic Seebeck Effect in Conducting Polymers. *Adv. Energy Mater.* **2015**, *5*, 1500044.

(20) Wieland, M.; Dingler, C.; Merkle, R.; Maier, J.; Ludwigs, S. Humidity-Controlled Water Uptake and Conductivities in Ion and Electron Mixed Conducting Polythiophene Films. *ACS Appl. Mater. Interfaces* **2020**, *12*, 6742−6751.

(21) Li, H.; Lian, F.; Meng, N.; Xiong, C.; Wu, N.; Xu, B.; Li, Y. Constructing Electronic and Ionic Dual Conductive Polymeric Interface in the Cathode for High-Energy-Density Solid-State Batteries. *Adv. Funct. Mater.* **2021**, *31*, 2008487.

(22) del Olmo, R.; Mendes, T. C.; Forsyth, M.; Casado, N. Mixed Ionic and Electronic Conducting Binders Containing PEDOT:PSS and Organic Ionic Plastic Crystals toward Carbon-Free Solid-State Battery Cathodes. *J. Mater. Chem. A* **2022**, *10*, 19777−19786.

(23) Stavrinidou, E.; Leleux, P.; Rajaona, H.; Khodagholy, D.; Rivnay, J.; Lindau, M.; Sanaur, S.; Malliaras, G. G. Direct Measurement of Ion Mobility in a Conducting Polymer. *Adv. Mater.* **2013**, *25*, 4488−4493.

(24) Rivnay, J.; Inal, S.; Collins, B. A.; Sessolo, M.; Stavrinidou, E.; Strakosas, X.; Tassone, C.; Delongchamp, D. M.; Malliaras, G. G. Structural Control of Mixed Ionic and Electronic Transport in Conducting Polymers. *Nat. Commun.* **2016**, *7*, 11287.

(25) Lyu, D.; Jin, Y.; Magusin, P. C. M. M.; Sturniolo, S.; Zhao, E. W.; Yamamoto, S.; Keene, S. T.; Malliaras, G. G.; Grey, C. P. Operando NMR Electrochemical Gating Studies of Ion Dynamics in PEDOT:PSS. *Nat. Mater.* **2023**, *22*, 746−753.

(26) Zozoulenko, I.; Singh, A.; Singh, S. K.; Gueskine, V.; Crispin, X.; Berggren, M. Polarons, Bipolarons, And Absorption Spectroscopy of PEDOT. *ACS Appl. Polym. Mater.* **2019**, *1*, 83−94.

(27) Balooch Qarai, M.; Ghosh, R.; Hestand, N. J.; Spano, F. C. Multipolaron Complexes in Conducting Polymers: The Importance

of Hole−Hole Repulsion in Charge Delocalization. *J. Phys. Chem. C* **2023**, *127*, 6414−6424.
(28) Franco-Gonzalez, J. F.; Zozoulenko, I. V. Molecular Dynamics Study of Morphology of Doped PEDOT: From Solution to Dry Phase. *J. Phys. Chem. B* **2017**, *121*, 4299−4307.
(29) Modarresi, M.; Franco-Gonzalez, J. F.; Zozoulenko, I. Morphology and Ion Diffusion in PEDOT:Tos. A Coarse Grained Molecular Dynamics Simulation. *Phys. Chem. Chem. Phys.* **2018**, *20*, 17188−17198.
(30) Modarresi, M.; Franco-Gonzalez, J. F.; Zozoulenko, I. Computational Microscopy Study of the Granular Structure and PH Dependence of PEDOT:PSS. *Phys. Chem. Chem. Phys.* **2019**, *21*, 6699−6711.
(31) Modarresi, M.; Mehandzhiyski, A.; Fahlman, M.; Tybrandt, K.; Zozoulenko, I. Microscopic Understanding of the Granular Structure and the Swelling of PEDOT:PSS. *Macromolecules* **2020**, *53*, 6267−6278.
(32) de Izarra, A.; Choi, C.; Jang, Y. H.; Lansac, Y. Molecular Dynamics of PEDOT:PSS Treated with Ionic Liquids. Origin of Anion Dependence Leading to Cation Design Principles. *J. Phys. Chem. B* **2021**, *125*, 8601−8611.
(33) Khot, A.; Savoie, B. M. Top−Down Coarse-Grained Framework for Characterizing Mixed Conducting Polymers. *Macromolecules* **2021**, *54*, 4889−4901.
(34) Makki, H.; Troisi, A. Morphology of Conducting Polymer Blends at the Interface of Conducting and Insulating Phases: Insight from PEDOT:PSS Atomistic Simulations. *J. Mater. Chem. C* **2022**, *10*, 16126−16137.
(35) Yildirim, E.; Wu, G.; Yong, X.; Tan, T. L.; Zhu, Q.; Xu, J.; Ouyang, J.; Wang, J.-S.; Yang, S.-W. A Theoretical Mechanistic Study on Electrical Conductivity Enhancement of DMSO Treated PEDOT:PSS. *J. Mater. Chem. C* **2018**, *6*, 5122−5131.
(36) Modarresi, M.; Zozoulenko, I. Why Does Solvent Treatment Increase the Conductivity of PEDOT : PSS? Insight from Molecular Dynamics Simulations. *Phys. Chem. Chem. Phys.* **2022**, *24*, 22073−22082.
(37) de Izarra, A.; Choi, C.; Jang, Y. H.; Lansac, Y. Ionic Liquid for PEDOT:PSS Treatment. Ion Binding Free Energy in Water Revealing the Importance of Anion Hydrophobicity. *J. Phys. Chem. B* **2021**, *125*, 1916−1923.
(38) Franco-Gonzalez, J. F.; Rolland, N.; Zozoulenko, I. V. Substrate-Dependent Morphology and Its Effect on Electrical Mobility of Doped Poly(3,4-Ethylenedioxythiophene) (PEDOT) Thin Films. *ACS Appl. Mater. Interfaces* **2018**, *10*, 29115−29126.
(39) Genovese, C.; Antidormi, A.; Dettori, R.; Caddeo, C.; Mattoni, A.; Colombo, L.; Melis, C. Linking Morphology to Thermal Conductivity in PEDOT: An Atomistic Investigation. *J. Phys. D: Appl. Phys.* **2017**, *50*, 494002.
(40) Shi, W.; Zhao, T.; Xi, J.; Wang, D.; Shuai, Z. Unravelling Doping Effects on PEDOT at the Molecular Level: From Geometry to Thermoelectric Transport Properties. *J. Am. Chem. Soc.* **2015**, *137*, 12929−12938.
(41) Floris, P. S.; Melis, C.; Rurali, R. Interplay Between Doping, Morphology, and Lattice Thermal Conductivity in PEDOT:PSS. *Adv. Funct. Mater.* **2023**, *33*, 2215125.
(42) Rolland, N.; Franco-Gonzalez, J. F.; Volpi, R.; Linares, M.; Zozoulenko, I. V. Understanding Morphology-Mobility Dependence in PEDOT:Tos. *Phys. Rev. Mater.* **2018**, *2*, 045605.
(43) Rolland, N.; Franco-Gonzalez, J. F.; Zozoulenko, I. Can Mobility Negative Temperature Coefficient Be Reconciled with the Hopping Character of Transport in Conducting Polymers? *ACS Appl. Polym. Mater.* **2019**, *1*, 2833−2839.
(44) Keene, S. T.; Michaels, W.; Melianas, A.; Quill, T. J.; Fuller, E. J.; Giovannitti, A.; McCulloch, I.; Talin, A. A.; Tassone, C. J.; Qin, J.; Troisi, A.; Salleo, A. Efficient Electronic Tunneling Governs Transport in Conducting Polymer-Insulator Blends. *J. Am. Chem. Soc.* **2022**, *144*, 10368−10376.
(45) Alessandri, R.; Grünewald, F.; Marrink, S. J. The Martini Model in Materials Science. *Adv. Mater.* **2021**, *33*, 2008635.
(46) Marrink, S. J.; Monticelli, L.; Melo, M. N.; Alessandri, R.; Tieleman, D. P.; Souza, P. C. T. Two Decades of Martini: Better Beads, Broader Scope. *Wiley Interdiscip. Rev.: Comput. Mol. Sci.* **2023**, *13*, No. e1620.
(47) Souza, P. C. T.; Alessandri, R.; Barnoud, J.; Thallmair, S.; Faustino, I.; Grünewald, F.; Patmanidis, I.; Abdizadeh, H.; Bruininks, B. M. H.; Wassenaar, T. A.; Kroon, P. C.; Melcr, J.; Nieto, V.; Corradi, V.; Khan, H. M.; Domański, J.; Javanainen, M.; Martinez-Seara, H.; Reuter, N.; Best, R. B.; Vattulainen, I.; Monticelli, L.; Periole, X.; Tieleman, D. P.; de Vries, A. H.; Marrink, S. J. Martini 3: A General Purpose Force Field for Coarse-Grained Molecular Dynamics. *Nat. Methods* **2021**, *18*, 382−388.
(48) Kim, D.; Zozoulenko, I. Why Is Pristine PEDOT Oxidized to 33%? A Density Functional Theory Study of Oxidative Polymerization Mechanism. *J. Phys. Chem. B* **2019**, *123*, 5160−5167.
(49) Kim, D.; Franco-Gonzalez, J. F.; Zozoulenko, I. How Long Are Polymer Chains in Poly(3,4-Ethylenedioxythiophene):Tosylate Films? An Insight from Molecular Dynamics Simulations. *J. Phys. Chem. B* **2021**, *125*, 10324−10334.
(50) Jain, K.; Mehandzhiyski, A. Y.; Zozoulenko, I.; Wågberg, L. PEDOT:PSS Nano-Particles in Aqueous Media: A Comparative Experimental and Molecular Dynamics Study of Particle Size, Morphology and z-Potential. *J. Colloid Interface Sci.* **2021**, *584*, 57−66.
(51) Humphrey, W.; Dalke, A.; Schulten, K. VMD: Visual Molecular Dynamics. *J. Mol. Graph.* **1996**, *14*, 33−38.
(52) Rossi, G.; Monticelli, L.; Puisto, S. R.; Vattulainen, I.; Ala-Nissila, T. Coarse-Graining Polymers with the MARTINI Force-Field: Polystyrene as a Benchmark Case. *Soft Matter* **2011**, *7*, 698−708.
(53) Panizon, E.; Bochicchio, D.; Monticelli, L.; Rossi, G. MARTINI Coarse-Grained Models of Polyethylene and Polypropylene. *J. Phys. Chem. B* **2015**, *119*, 8209−8216.
(54) Grunewald, F.; Rossi, G.; de Vries, A. H.; Marrink, S. J.; Monticelli, L. Transferable MARTINI Model of Poly(Ethylene Oxide). *J. Phys. Chem. B* **2018**, *122*, 7436−7449.
(55) Alessandri, R.; Souza, P. C. T.; Thallmair, S.; Melo, M. N.; de Vries, A. H.; Marrink, S. J. Pitfalls of the Martini Model. *J. Chem. Theory Comput.* **2019**, *15*, 5448−5460.
(56) Rolland, N.; Modarresi, M.; Franco-Gonzalez, J. F.; Zozoulenko, I. Large Scale Mobility Calculations in PEDOT (Poly(3,4-Ethylenedioxythiophene)): Backmapping the Coarse-Grained MARTINI Morphology. *Comput. Mater. Sci.* **2020**, *179*, 109678.
(57) Abraham, M. J.; Murtola, T.; Schulz, R.; Páll, S.; Smith, J. C.; Hess, B.; Lindahl, E. GROMACS: High Performance Molecular Simulations through Multi-Level Parallelism from Laptops to Supercomputers. *SoftwareX* **2015**, *1−2*, 19−25.
(58) Bauer, P.; Hess, B.; Lindahl, E. *GROMACS 2022.2 Source Code*, 2022.
(59) Bussi, G.; Donadio, D.; Parrinello, M. Canonical Sampling through Velocity Rescaling. *J. Chem. Phys.* **2007**, *126*, 014101.
(60) Berendsen, H. J. C.; Postma, J. P. M.; van Gunsteren, W. F.; DiNola, A.; Haak, J. R. Molecular Dynamics with Coupling to an External Bath. *J. Chem. Phys.* **1984**, *81*, 3684−3690.
(61) Parrinello, M.; Rahman, A. Polymorphic Transitions in Single Crystals: A New Molecular Dynamics Method. *J. Appl. Phys.* **1981**, *52*, 7182−7190.
(62) Essmann, U.; Perera, L.; Berkowitz, M. L.; Darden, T.; Lee, H.; Pedersen, L. G. A Smooth Particle Mesh Ewald Method. *J. Chem. Phys.* **1995**, *103*, 8577−8593.
(63) Skånberg, R.; Linares, M.; König, C.; Norman, P.; Jönsson, D.; Hotz, I.; Ynnerman, A. VIA-MD: Visual Interactive Analysis of Molecular Dynamics. *Workshop on Molecular Graphics and Visual Analysis of Molecular Data*, 2018; p 9.
(64) Skanberg, R.; Falk, M.; Linares, M.; Ynnerman, A.; Hotz, I. Tracking Internal Frames of Reference for Consistent Molecular Distribution Functions. *IEEE Trans. Vis. Comput. Graph.* **2022**, *28*, 3126−3137.

(65) Markutsya, S.; Lamm, M. H. A Coarse-Graining Approach for Molecular Simulation That Retains the Dynamics of the All-Atom Reference System by Implementing Hydrodynamic Interactions. *J. Chem. Phys.* **2014**, *141*, 174107.
(66) Samson, E.; Marchand, J.; Snyder, K. A. Calculation of Ionic Diffusion Coefficients on the Basis of Migration Test Results. *Mat. Struct.* **2003**, *36*, 156−165.
(67) Stavrinidou, E.; Leleux, P.; Rajaona, H.; Fiocchi, M.; Sanaur, S.; Malliaras, G. G. A Simple Model for Ion Injection and Transport in Conducting Polymers. *J. Appl. Phys.* **2013**, *113*, 244501.

https://doi.org/10.1021/acs.chemmater.3c00873
Chem. Mater. 2023, 35, 5512−5523